Spurious Free Dynamic Range for a Digitizing Array

Langford B. White, *Senior Member, IEEE*, Feng Rice, and Angus Massie, *Member, IEEE*

***Abstract*—This paper addresses the problem of improving the spurious free dynamic range (SFDR) for digitization by use of antenna arrays. Nonlinearities in the analog-to-digital conversion process give rise to spurious signals (harmonics and intermodulation products) that limit the overall SFDR of the digitization process. When the signal of interest arises from a sensor such as an antenna or hydrophone, the paper addresses the question of whether array processing (ie use of multiple antennas) can improve the resulting SFDR at the beamformer output. The paper argues that significant improvements can be obtained using linear, or more effectively, optimal (minimum variance distortionless response) beamforming.**

***Index Terms*—Analog-to-digital conversion, array processing, digital receivers, spurious free dynamic range.**

I. Introduction

THE use of sensor arrays has become widespread in areas such as sonar, radar and, wireless communications, to name but a few. The main benefits of using sensor arrays rather than a single sensor is to exploit the spatial separation of energy impinging on the array. For example, one may wish to find the direction of arrival (DOA) of a specific signal, or alternatively, one may seek to improve the signal-to-noise ratio (SNR) of a desired signal by using the spatial selectivity offered by a sensor array to enhance the desired signal while simultaneously attenuating undesired signals present in the same passband but having a different DOA.

This paper in concerned with a perhaps not as widely understood, yet beneficial, effect of using sensor arrays when viewed from the point of view of signal digitization. The analog-to-digital conversion process is inherently a nonlinear operation. The deficiencies of practical devices and the deleterious effects caused the signal distortion have been studied by many including [1] and [5]. These nonidealities in the analog-to-digital conversion process can degrade the receiver sensitivity due primarily to the production of intermodulation distortion components that limit the useful dynamic range of the analog-to-digital converter (ADC) [4], resulting in a drop in overall system performance. Antenna arrays suffer the same problem [3] with distortion since for digital beamforming, an ADC is used to first digitize the signals from each array sensor. Early research results have revealed that the linear beamformer has low capacities to cope with ADC nonlinearities [1] and [2]. These results examine *inter alia* the effect on the beampattern of ADC nonlinearities. However, in the case of a digitising array as shown in Fig. 1, spurious signals introduced by the ADC appear at a different location in the frequency-wavenumber space to the desired component [4]. This property has motivated us to investigate spatial filters (beamformers) that may remove and/or suppress these undesirable byproducts of the nonideal ADC behavior. Our measure of the fidelity of the process will be the spurious free dynamic range (SFDR) at the output of the beamformer. We also make reference to [6], which addresses the converse problem of spatially characterizing the spurious signals caused by power amplifier nonlinearities in a transmitter antenna array.

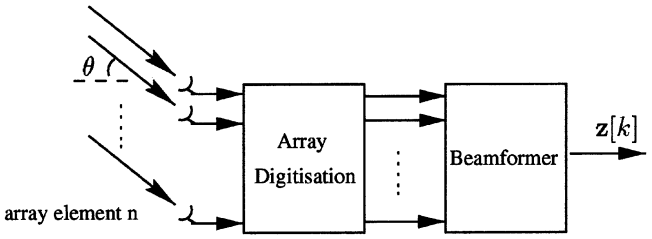

Fig. 1. Linear equispaced array with beamformer.

In Section II, we present the signal processing model used for analysis. Section III explains the principles of spatial-temporal filtering, which be used to suppress distortion products and improve the SFDR. The ADC nonlinear model is described in Section IV, and a Fourier series representation for the ADC output for a narrowband input is derived. This series representation permits an analytic calculation of the SFDR improvement, which can be gained due to the spatial filtering. We discuss optimal beamforming in Section V, and simulation results using multiple input signals are presented in Section VI. We believe that this work represents the first attempt to exploit the spatio-temporal properties of the ADC distortion products by spatial filtering (beamforming) in order to improve overall SFDR.

II. Signal Processing Model

Fig. 2 shows the signal processing model under study. Each array sensor signal is passed through an analog anti-aliasing filter with cutoff frequency of $f_s/2$, where f_s is the ADC sampling rate. The sampled signals at the ADC output are then quadrature downmixed with local oscillator frequency f_o and lowpass filtered using a digital filter with transfer function

Manuscript received June 12, 2002; revised March 20, 2003. This work was supported by the Communications Division of Defence Science and Technology Organization of Australia. The associate editor coordinating the review of this paper and approving it for publication was Dr. Rick S. Blum.

L. B. White is with the Department of Electrical and Electronic Engineering, Adelaide University, Adelaide 5005 SA, Australia (e-mail : Lang.White@adelaide.edu.au).

F. Rice is with Cooperative Research Center for Sensor Signal and Information Processing, Department of Electrical and Electronic Engineering, Adelaide University, Adelaide 5005 SA, Australia (feng@cssip.edu.au).

A. Massie is with the Communications Division, Defence Science and Technology Organization, Salisbury SA, Australia.

Digital Object Identifier 10.1109/TSP.2003.819003

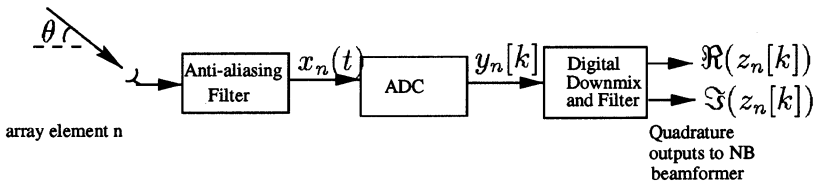

Fig. 2. Signal processing model for array digitization.

$H(f)$. These complex baseband signals from each sensor are then combined using a beamformer.

Suppose, for the sake of simplicity, that we restrict our attention to linear, equispaced arrays. We consider an array with N isotropic sensors, where each is separated by d m. The response at sensor n to a single narrowband plane wave incident at wavenumber ν ($= \sin\theta$, where θ is the incident azimuth angle) with carrier frequency f Hz is

$$x_n(t) = \Re\left(s(t)\, e^{i2\pi f(t+n\nu d/c)}\right) \tag{1}$$

where $s(t)$ is the baseband modulation on the signal, and c denotes the wave propagation speed in meters per second, In the paper, we will assume continuous wave modulation with $s(t) = A$ for some constant $A > 0$.

Each sensor signal is passed through an identical ADC, which we represent by the operator $\mathcal{H}$. We will discuss a typical models for the ADC process in Section IV. The sample rate is given by f_s Hz. The output of the ADC for sensor n is thus

$$y_n[k] = \mathcal{H}(x_n)\left(\frac{k}{f_s}\right) \tag{2}$$

for $k \geq 0$. Each signal is quadrature downmixed with oscillator frequency f_0, and (lowpass) filter impulse response coefficients $h[k]$, $k \geq 0$, yielding

$$z_n[k] = \sum_{\ell\geq 0} h[\ell]\, y_n[k-\ell]\, e^{-2\pi i(k-\ell)f_0/f_s}. \tag{3}$$

These signals are combined using a beamformer

$$z[k] = \sum_{n=0}^{N-1} g_n(f_0\nu_0)\, z_n[k] \tag{4}$$

where g_n are the beamformer weights. Here, ν_0 is the wavenumber of the desired signal. For a conventional linear beamformer, we have

$$g_n(\beta) = w_n\, e^{-2\pi i n\beta d/c} \tag{5}$$

where the $w_n, n = 0, \ldots, N-1$ are real windowing (or shading) coefficients chosen to tradeoff main lobe width and side lobe levels. It is often useful to define the *spatial-temporal array response*

$$W(\beta) = \sum_{n=0}^{N-1} w_n\, e^{-2\pi i n\beta d/c} \tag{6}$$

which is a periodic function with period c/d. Fig. 3 shows the array responses for a $N = 10$ element array with $d = 10$ m, $T = 1000$ samples, and $w_n = 1/N$ for the linear beamforming and the optimum beamforming response, which we discuss in Section V. Notice that the beamformer response is a function of the product $\beta = f_o\,\nu_o$ of the frequency and spatial frequency. It is this property that we exploit in order to improve the SFDR at the output. In this example, we have used uniform weights on the antenna array, resulting in the familiar sidelobe patterns. Of course, much work has been conducted in the selection of window coefficients for both arrays and FIR time domain digital filters, and other weight distributions could be used to obtain the usual tradeoffs between main lobe width and sidelobe levels. We do not address this issue in this paper but note that different choices of windows will yield different SFDR results.

A. Response for Ideal ADC

Consider the case where the ADC process is ideal, i.e., $\mathcal{H}$ is the identity operator, and $s(t) = A$. Then, from (1) to (5), we obtain (7), shown at the bottom of the page.

Thus

$$z[k] = \frac{A}{2}\Big[e^{-i2\pi(f_0-f)k/f_s}H(f-f_0)W(f_0\nu_0 - f\nu) + e^{-i2\pi(f+f_0)k/f_s}H(-f-f_0)W(f_0\nu_0 + f\nu)\Big]. \tag{8}$$

If the incident signal was indeed the desired signal, then we set $f_0 = f$ and $\nu_0 = \nu$, yielding

$$z[k] = \frac{A}{2}\left[H(0)W(0) + e^{-i4\pi fk/f_s}H(-2f)W(2f\nu)\right]. \tag{9}$$

Typically, the lowpass filter cutoff is chosen so that $H(-2f)$ is negligible, and we scale the lowpass filter ($h[k]$) and beamformer (w_n) coefficients so that $H(0) = 2$ and $W(0) = 1$, thus yielding unit response to the desired signal.

$$\begin{aligned} z[k] &= \sum_{n=0}^{N-1}\sum_{\ell\geq 0} h[\ell]\, w_n\, e^{-i2\pi f_0((k-\ell)/f_s + n\nu_0 d/c)}\, A\,\Re\left(e^{i2\pi f((k-\ell)/f_s + n\nu d/c)}\right) \\ &= \frac{A}{2}\sum_{n=0}^{N-1}\sum_{\ell\geq 0} h[\ell]\, w_n\, \left[e^{-i2\pi(f_0-f)(k-\ell)/f_s}\, e^{-i2\pi nd/c(f_0\nu_0 - f\nu)} + e^{-i2\pi(f_0+f)(k-\ell)/f_s}\, e^{-i2\pi nd/c(f_0\nu_0 + f\nu)}\right]. \end{aligned} \tag{7}$$

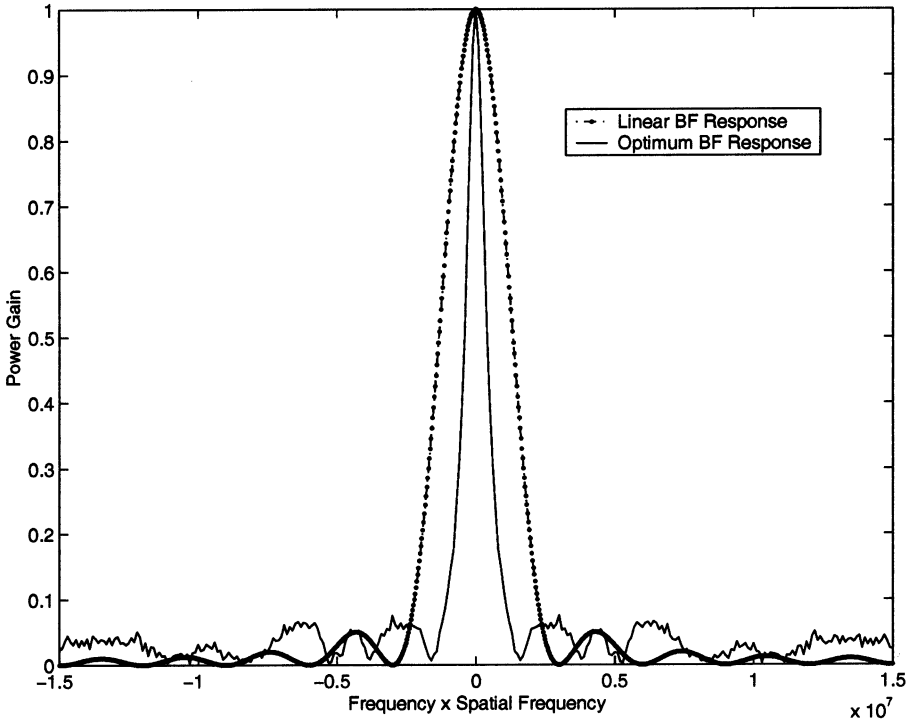

Fig. 3. Beamforming responses.

III. Spatial-Temporal Aliasing

As pointed out earlier, we process the received array signals in both the temporal and spatial domain. The temporal sampling is performed at rate f_s; therefore, temporal aliasing will occur with period f_s. Spatial sampling is performed by the sensor array, with spatial aliasing occurring with the spatio-temporal (i.e., in the product $\beta = f\nu$) period c/d. When the harmonic or intermodulation signal terms have a frequency or spatio-temporal product β that exceeds half the relevant sample rate, they are folded back in the fundamental region. The fundamental region is defined as the region for which the spatial frequency-wavenumber product $\beta \in [-c/2d, c/2d]$, and the temporal frequency $f \in [-f_s/2, f_s/2]$. Note we only show positive temporal frequencies in Fig. 4, which illustrates the aliasing and the invisible region. Here, f_c is the cut-off frequency of the (digital) lowpass filter. The aliasing region is defined to be all values of (f, β) that are outside the fundamental region. The visible region is defined to be that area that corresponds to $-1 \leq \sin\theta \leq 1$. The dashed line with wavenumber $\nu = \pm 1$ shown as OA and OB splits the fundamental region into two regions—the visible region and the invisible region. The invisible region has spatial frequencies that do not correspond to any physically valid arrival angle on the array; however, as we will see, distortion terms from the ADC can fall in this region.

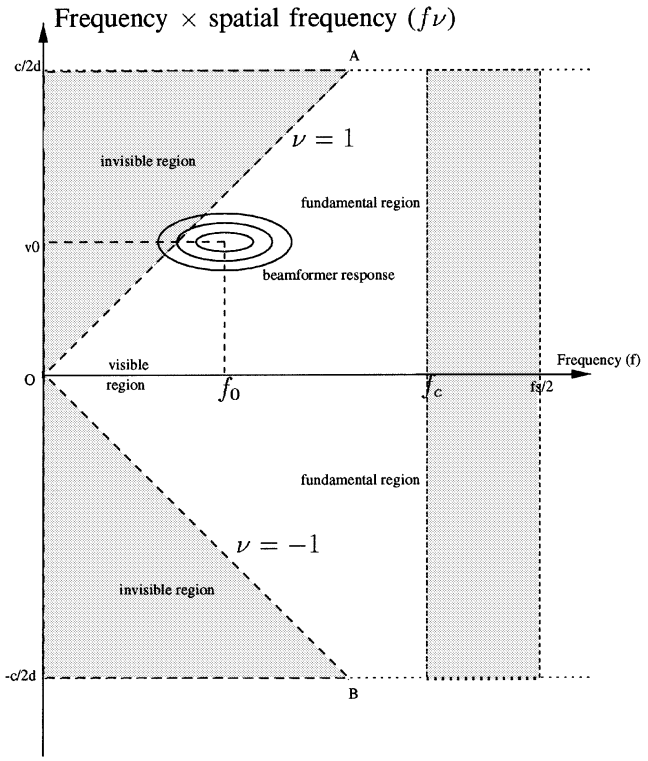

Fig. 4. Spatio-temporal aliasing and the invisible regions.

IV. Nonlinear ADC Model

In this section, we derive a Fourier series representation for the output of an ADC when the input is a single narrowband signal. This representation is useful for determining the SFDR improvement analytically. All ADCs possess nonlinearities due to the nonideal sample, hold operation and amplifier nonlinearities. We consider only one model of such imperfections, which has been studied in [5]

$$\Lambda[x(t)] = x(t) + \gamma \dot{x}(t)\,[M - |x(t)|] \tag{10}$$

where M is the maximum modulus of $x(t)$, γ is a measure of the departure from linearity, and $\dot{x}$ denotes the derivative of x.

Larger values of γ will give rise to increased distortion, and the Appendix contains a derivation of the SFDR at the output of the ADC (for a narrowband input) in terms of γ. This model is desirable since it does not depend explicitly on the type or parameters associated with the signal. We note that there are many possible models for ADC nonlinearities, and we refer interested readers to [5] as well as [1] and [2] for more detailed discussion. We comment that for any realistic model, we expect to see the presence of harmonics and intermodulation distortion products in the output, and while our quantitative results are valid only for the model considered, we argue that the general qualitative conclusions regarding the ability of array processing to suppress the level of such distortion terms remains valid for other such ADC models.

For narrowband inputs (i.e., sinusoids), the output consists of a harmonic series of sinusoids at multiples of the input frequency. In general, for input $x_n(t) = A\cos(2\pi f(t+\tau_n))$, the ADC output is given as

$$\begin{aligned}\Lambda[A\cos(2\pi f(t+\tau_n))] =& A\cos(2\pi f(t+\tau_n)) \\ &- 2\pi f A^2\gamma\sin(2\pi f(t+\tau_n)) \\ &\cdot(1-|\cos(2\pi f(t+\tau_n)|). \quad (11)\end{aligned}$$

The Appendix derives the complex Fourier series coefficients for the signal (11) when $\tau_n = 0$. The output of the ADC is

$$\begin{aligned}y_n(t) = A\cos(2\pi ft) &- 2\pi\gamma f A^2\delta_1\sin(2\pi ft) \\ &-2\pi\gamma f A^2\sum_{k=2}^{\infty}\delta_k\ \sin(2\pi ft(2k-1)) \quad (12)\end{aligned}$$

where the δ_k terms are defined in the Appendix. This permits SFDR expressions to be obtained at the input and output of the beamformer. In Section VI-A, we present a comparison between these theoretical expressions and simulation results.

When there are multiple input signals, a series representation for the ADC output becomes complicated due to the interaction terms between the various signal components. However, in principle, a frequency domain description can be found. For our experiments, we used simulations to determine the SFDR improvement when multiple inputs are present.

V. Optimal Beamforming

The minimum variance distortionless response (MVDR) beamformer is an optimal approach to the beamforming problem [7]. In this approach, the beamformer response is constrained to unity (hence *distortionless*) in the desired direction, and the total output power (*variance*) is minimized. Our objective is to use the output of the quadrature downmix to specify the beamformer weights g_n. Assuming the carrier frequency f and the wavenumber ν, the elements of the array steering N-vector μ are defined by

$$\mu_n(\beta) = e^{-2\pi i dn\beta/c}, \quad n = 0, 1, \ldots N-1. \quad (13)$$

We choose g_n by fixing the gain as unity for desired $\beta = f_0\nu_0$ and minimizing the total output power. The solution for the weight vector $g = [g_0, \ldots, g_{N-1}]^T$ is given by

$$g = \frac{R_z^{-1}\mu(f_0\nu_0)}{\mu^H(f_0\nu_0)R_z^{-1}\mu(f_0\nu_0)} \quad (14)$$

where R_z is the estimated $N\times N$ array data (after ADC and the down-conversion) covariance matrix

$$[R_z]_{nm} = \frac{1}{T}\sum_{k=1}^{T} z_n[k]\, z_m^*[k] \quad (15)$$

for some block of data of length of T samples. Here, ^{H} denotes conjugate transpose, and * denotes conjugation. The optimum beamforming response is plotted in Fig. 3, together with the linear beamforming response for a single incident signal at angle 0. The optimum array response is much sharper than the linear one, although sidelobes are higher in this particular example. This illustrates the potential ability of the MVDR beamformer to filter out closely spaced signals in the spatial domain.

VI. Simulation Results

We wish to compare the effect of the beamforming operation in terms of suppression of undesirable signal components introduced by the ADC nonidealities. In our simulations, we applied the input signal(s) to the ADC model (in sampled form) and then to a quadrature downmix (from Matlab) filter. The relevant beamformer (linear or MVDR) was also coded in Matlab. We will assume that the quadrature downmix local oscillator frequency f_o is set to the carrier frequency of the desired signal and that the beamformer parameter β is set to the product $f_o\nu_o$ of the desired signal carrier frequency and wavenumber. The SFDR will be defined as the ratio of the power of the desired signal component to the power of the next largest term at the beamformer output when all signals have equal power. Clearly, this will depend on the bandwidth of the lowpass filter $H(f)$. In practice, one would set the bandwidth of H suitably small to cover just the passband of the signal of interest. We will set the bandwidth of H variously between 0.10 and 0.35 of the sampling frequency f_s in our experiments in order to illustrate the benefits of our approach. This is still a realistic situation since in a very dense signal environment such as is found in the HF bands, there still remains a high probability of distortion products appearing in the chosen passband.

A. Single Incident Signal

Consider a single incident on a uniform linear array with ten elements and the array spacing $d = 10$ m. We assume that the baseband transmitted signal is a constant $s(t) = 1$, with carrier frequency $f_0 = 10$ MHz, the arrival angle $\theta = \pi/6$, the sample rate $f_s = 36$ MHz, and the anti-aliasing filter cut-off frequency $f_c = 0.35\, f_s$. Aliased harmonics are shown in Table I together with the comparison of the calculated SFDR [using the Fourier series representation (12)] and simulated results obtained using

TABLE I
SFDR IMPROVEMENT FOR A SINGLE SIGNAL

Signal Components	Signal	Harmonics		
	1	3	5	7
Frequency (MHz) - f	10	-6	14	-2
$\beta = f\nu$	5	15	-5	5
Location	Visible	Invisible	Visible	Visible
Theoretical SFDR (dB)				
Before Beamforming	0	35.9	48.4	58.4
Linear Beamforming	0	51.2	63.6	74.1
Simulated SFDR (dB)				
Before Beamforming	0	36.2	49.8	59.4
Linear Beamforming	0	50.9	60.0	79.4

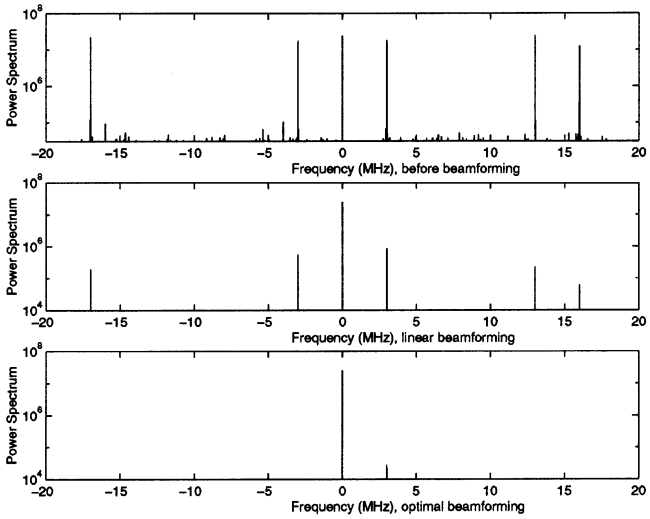

Fig. 5. Power spectra before beamforming and after linear and optimal beamforming.

a Matlab implementation of the system [incorporating the ADC model (10)]. We used $\gamma = 10^{-10}$.

Table I shows a good agreement between the theoretical calculation and the simulated results. The third-order term is located on the border of the invisible region. The linear beamforming increases SFDR over 10 dB in both measurements. The simulation results also show that the performance of the optimum beamformer is similar to that of the linear beamformer.

B. Multiple Incident Signals

Multiple incidents signals were simulated with carrier frequencies $f_1 = 7$ MHz, $f_2 = 10$ MHz, and $f_3 = 13$ MHz and corresponding arrival angles $\theta_1 = \pi/4$, $\theta_2 = \pi/3$, and $\theta_3 = \pi/9$. Each carrier had unit amplitude. The sample rate f_s was 36 MHz, and the antialiasing filter cut-off frequency was $0.1\,f_s$. The linear equispaced array has ten elements and array spacing $d = 10$ m. We assumed that the ADC nonlinearity factor was $\gamma = 10^{-10}$. The desired signal was at $f_0 = 10$ MHz with the arrival angle $\theta = \pi/3$. Complex additive white Gaussian noise was added to the signal at SNR= 9 dB. Here, SNR is defined to be $-10\log_{10}\sigma^2$, where σ^2 is the variance of the noise added to each quadrature signal component.

Fig. 5 shows the power spectrum of one sensor signal before beamforming and the power spectrum of the beamformer outputs, both linear and optimal. The SFDR is -0.25 dB before the any beamforming, SFDR=14.86 dB for the linear beamformer output, and SFDR $= 30.32$ dB for the optimum beamformer output. The performance of the optimum beamformer is superior to that of the linear beamformer by around 10 dB. We then varied the desired arrival direction ν_o only and kept other parameters unchanged. The simulation results are shown in Fig. 6. A clear degradation is evident in the region around $\nu_0 = 0.48$ corresponding to $\beta = 4.8 \times 10^6$. This degradation is due to the presence of the fundamental components of the other two signals at $f\nu = 4.94 \times 10^6$, 4.45×10^6. The optimal beamformer appears to maximize SFDR at the desired $f\nu = 0.866 \times 10^6$.

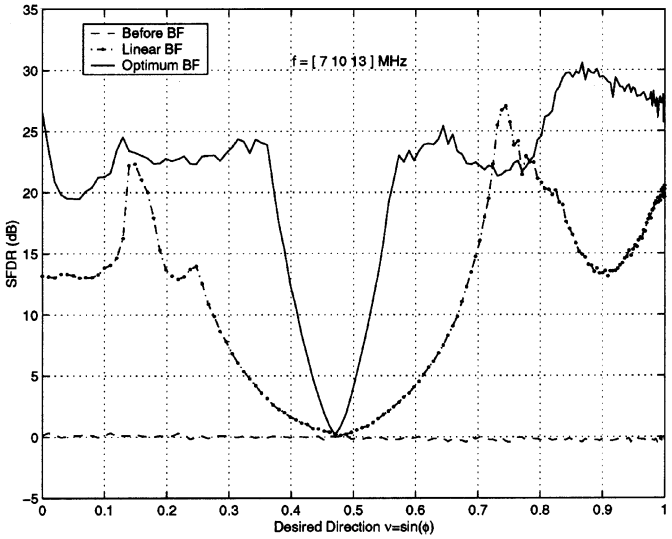

Fig. 6. Comparison of performance of the beamformers for three incident signals.

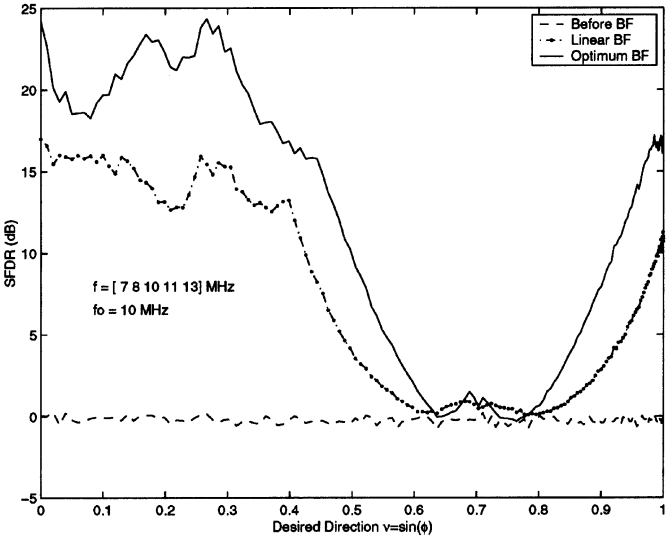

Fig. 7. Comparison of performance of the beamformers for five incident signals.

The similar simulation has been expanded to five carriers $\mathbf{f} = [7, 8, 10, 11, 13]$ MHz and the arrival angles $\boldsymbol{\theta} = [\pi/3, \pi/2, 0, \pi/4, \pi/6]$. The desired carrier frequency is 10 MHz, and the desired direction is 0. The other parameters are the same as in Fig. 5. The simulated results are shown in Fig. 7.

TABLE II
SFDR VALUES FOR VARYING NONLINEARITY PARAMETER, $f_o = 10$ MHz, $\theta = \pi/6$

$-\log_{10}\gamma$	5	7	8	9	10	15
SFDR (dB) (no b/f)	6.9	7.2	16.3	34.9	41.7	42.0
SFDR (dB) (Linear)	19.6	19.9	29.0	47.5	53.5	53.8
SFDR (dB) (MVDR)	20.4	20.8	29.4	39.4	42.0	40.1

The simulation results reveal that the performance of the optimum beamformer is generally better than that of the linear beamformer by a few decibels to over 20 dB, depending on the signal scenario. Performance is again poor in the region $\beta = 0.6$ to 0.8. This is because the fundamental terms of the other signals are at $f\nu = 6.06 \times 10^6$, 6.5×10^6, 7.78×10^6, and 8×10^6, corresponding to spatial frequencies of 0.606, 0.65, 0.778, and 0.8, respectively. In addition, many of the third-order interference terms lie in this spatial frequency band. In addition, we again note that the optimal beamformer maximizes SFDR at the location of the desired signal $\beta = 0$. We averaged SFDR across the range of ν_0 and found that the average SFDR was 7.02 dB for the linear beamforming and 11.66 dB for the optimum beamforming.

C. Effect of Varying the Nonlinearity Parameter

In this section, we varied the nonlinearity parameter γ in the model (10) over the range 10^{-5} to 10^{-15}. The resulting SFDRs obtained from the simulation for the five incident signals scenario as used above are shown in Table II.

These results illustrate that the performance of the MVDR beamformer is lower compared with the linear beamformer for lower levels of distortion components. We argue that this phenomenon is due to the process of determining the MVDR beamformer weights, which relies on estimation of the signal covariance matrix R_z. Since the distortion products are at such a low level, they do not have much effect on the resulting beamformer weights, as determined by (14). Generally, we expect the MVDR beamformer to place spatio-temporal nulls at the location of significant distortion products, but in this case, we argue that the distortion products are not present at sufficient levels to result in this behavior. Longer integration times T may be required to improve the relative performance of the MVDR beamformer for low levels of distortion products.

In these simulations, we have fixed the value the sampling and cut-off frequencies. Discussion concerning the choice of cut-off frequency for the filter is given above. The relative performance of each beamformer for different values of sampling frequency is highly dependent on the particular scenario of incident signals, and general conclusions cannot be made easily. However, higher sampling rates should reduce aliasing in general and thus increase attainable SFDR.

VII. CONCLUSION

We have investigated the applicability of sensor array processing in improving the spurious free dynamic range of the resulting digitised signal. We have demonstrated that significant suppression of spurious terms produced by nonidealities in the signal digitization process can be obtained by exploiting both their spatial and temporal frequency properties. Spatio-temporal filtering suppresses undesired spurious terms introduced by the imperfections in the analog-to-digital conversion process since these terms are generally found in different locations in the spatio-temporal coordinate space than the desired signals. Simulation results have compared the performance of the linear beamformer and the minimum variance distortionless response (MVDR) beamformer in terms of spurious free dynamic range (SFDR) improvement. These results indicate that the MVDR beamformer generally has superior performance to the linear beamformer, although for very low levels of distortion, the MVDR beamformer may perform comparatively worse.

APPENDIX
DERIVATION OF FOURIER SERIES COEFFICIENTS

Suppose the input to the ADC is $x(t) = A\cos(2\pi ft)$, then from (10), the ADC output is

$$\Lambda[x(t)] = A\cos(2\pi ft) - 2\pi f A^2 \gamma \sin(2\pi ft)\,(1 - |\cos(2\pi ft)|). \tag{16}$$

The function $|\cos(2\pi ft)|$ has the Fourier series representation

$$|\cos(2\pi ft)| = \sum_{k=-\infty}^{+\infty} c_k\, e^{4\pi ift} \tag{17}$$

where

$$c_k = \frac{2(-1)^{k+1}}{\pi(4k^2-1)}. \tag{18}$$

Thus

$$1 - |\cos(2\pi ft)| = \sum_{k=-\infty}^{+\infty} d_k\, e^{4\pi ift} \tag{19}$$

where

$$d_k = \begin{cases} 1 - c_0 & k = 0 \\ -c_k & k \neq 0 \end{cases}. \tag{20}$$

Thus

$$\begin{aligned} &\sin(2\pi ft)\ (1 - |\cos(2\pi ft)|) \\ &= \frac{1}{2i}\left(e^{2\pi ift} - e^{-2\pi ift}\right) \sum_{k=-\infty}^{+\infty} d_k\, e^{4\pi ift} \\ &= \frac{1}{2i} \sum_{k=-\infty}^{+\infty} d_k \left(e^{2\pi if t(2k+1)} - e^{2\pi if t(2k-1)}\right) \\ &= \frac{1}{2i} \sum_{k=-\infty}^{+\infty} e^{2\pi if(2k-1)}\,(d_{k-1} - d_k) \\ &= \sum_{k=1}^{\infty} \delta_k\, \sin\left(2\pi ft(2k-1)\right) \end{aligned} \tag{21}$$

where

$$\delta_k = \begin{cases} 1 + c_1 - c_0, & k = 1 \\ c_k - c_{k-1}, & k \geq 2. \end{cases} \tag{22}$$

Thus

$$\Lambda[x(t)] = A\cos(2\pi ft) - 2\pi\gamma f A^2\delta_1 \sin(2\pi ft) - 2\pi\gamma f A^2 \sum_{k=2}^{\infty} \delta_k \sin(2\pi ft(2k-1)). \quad (23)$$

The largest undesirable term here is the nonlinear term at the fundamental frequency f. Thus, the SFDR in decibels at the output of the ADC is given by

$$\text{SFDR} = -20\log_{10}\left(2\pi f\gamma\delta_1 A^2\right) \quad (24)$$

where $\delta_1 = 0.5756$. The SFDR at the output can be computed by weighting each term in (23) by the corresponding gains of the quadrature downmix filter and beamformer and selecting the ratio of the powers of the desired to second largest power signal.

ACKNOWLEDGMENT

The authors would like to acknowledge the helpful discussion with Dr. M. Rice on verification of the simulation results. They also thank the anonymous reviewers, whose advice has improved the paper considerably.

REFERENCES

[1] D. R. Ucci and R. G. Petriot, "The effects of ADC nonlinearities on digital beamformers," in *Conf. Rec. MILCOM Bridging the Gap, Interoperability, Survivability, Security*, vol. 1, 1989, pp. 279–283.

[2] J. Litva and T. K. Lo, *Digital Beamforming in Wireless Communications*. Norwood, MA: Artech House, 1996.

[3] S. L. Loyka, "The influence of electromagnetic environment on operation of active array antennas: Analysis and simulation techniques," *Antennas Propagat. Mag.*, vol. 41, no. 6, pp. 23–39, Dec. 1999.

[4] A. Massie, D. Taylor, J. Kitchen, L. Casey, and W. Marwood, "Enhancing the performance of direct digitising arrays with super-resolution and co-channel techniques," Commun. Div., DSTO, Tech. Rep., Saisbury, Australia, 1999.

[5] J. Tsimbinos and K. Lever, "Applications of higher-order statistics to modeling, identification and cancellation of nonlinear distortion in high-speed samplers and analogue-to-digital converters using the Volterra and Wiener models," in *Proc. IEEE Signal Processing Workshop Higher Order Statistics*, South Lake Tahoe, CA, 1993, pp. 379–383.

[6] C. Hemmi, "Pattern characteristics of harmonic and intermodulation products in broad-band active transmit arrays," *IEEE Trans. Antennas Propagat.*, vol. 50, pp. 858–865, June 2002.

[7] J. Capon, "High-resolution frequency-wavenumber spectrum analysis," *Proc. IEEE*, vol. 57, pp. 1408–1418, Aug. 1969.

Langford B. White (SM'00) received the B.Sc.(Math.), B.E.(Hons.), and Ph.D. (Elect. Eng.) degrees from the University of Queensland, Brisbane, Australia, in 1984, 1985, and 1989 respectively.

From 1986 to 1999, he worked for the Defence Science and Technology Organization, Salisbury, Australia. Since 1999, he has been a Professor with the School of Electrical and Electronic Engineering, The University of Adelaide, Adelaide, Australia, where he is also Director of the Centre for Internet Technology Research. His research interests include signal processing, control, telecommunications, and internet engineering.

Feng Rice received the B.Eng (Hons.) degree in electronic engineering from Shandong University of Technology, Jinan, China, the M.Phil. degree in information engineering from City University, London, U.K., in 1992, and the Ph.D. degree from the University of South Australia, Adelaide, in 2002.

In 1993, she worked in the biomedical engineering area at the Flinders University of South Autralia, Adelaide. From 1995 to 1996, she was a research engineer with the Institute for Telecommunications Research, University of South Australia. From 1996 to 2001, she consulted in the area of simulation and modeling of telecommunications systems for a number of organizations. Since 2001, she has been a research fellow with the Cooperative Research Centre for Sensor Signal and Information Processing, Department of Electrical and Electronic Engineering, University of Adelaide, Adelaide, Australia. Her current research interests are performance bounds and algorithms for frequency and phase estimation of digitally modulated signals and for target tracking.

Angus Massie (M'96) received the B.Sc. and B.E. degree from Adelaide University, Adelaide, Australia in 1980, the M.S. degree from George Mason University, Fairfax, VA, in 1999, and the M.B.A. degree from University of South Australia, Adelaide, in 2001.

He has been with the Defence Science Technology Organization, Salisbury, Australia, since 1980, where he is currently involved in work on digital receiver arrays and as the RF Hub leader. He is also a principle researcher with Adelaide University, on a project to build a high dynamic range ADC for use in a pre-emptive null steering ionosonde. He is also an adjunct Senior Lecturer at the University of South Australia, where his research interest is in decision making.